

Electronic Supplementary Information

Tuning emissive characteristics of TADF emitters by fusing heterocycle with acridine as donors: Highly efficient orange to red organic emitting diodes with EQE over 20%

*Tianheng Chen^{ab}, Chen-Han Lu,^c Chih-Wei Huang,^c Xuan Zeng^a, Jie Gao^a, Zhanxiang Chen^a, Yepeng Xiang^a, Weixuan Zeng^a, Zhongyan Huang^b, Shaolong Gong^a, Chung-Chih Wu^{*c} and Chuluo Yang^{*ab}*

T. Chen, X. Zeng, J. Gao, Z. Chen, Y. Xiang, W. Zeng, S. Gong and Prof. C. Yang

^aHubei Collaborative Innovation Center for Advanced Organic Chemical Materials, Hubei Key lab on Organic and Polymeric Optoelectronic Materials, Department of Chemistry, Wuhan University, Wuhan, 430072, P. R. China.

E-Mail: clyang@whu.edu.cn

T. Chen, Z. Huang and Prof. C. Yang

^bCollege of Materials Science and Engineering, Shenzhen University, Shenzhen 518060, China

C.-H. Lu, C.-W. Huang and Prof. C.-C. Wu

^cDepartment of Electrical Engineering, Graduate Institute of Electronics Engineering and Graduate Institute of Photonics and Optoelectronics, National Taiwan University, Taipei, 10617, Taiwan

E-mail: wucc@ntu.edu.tw

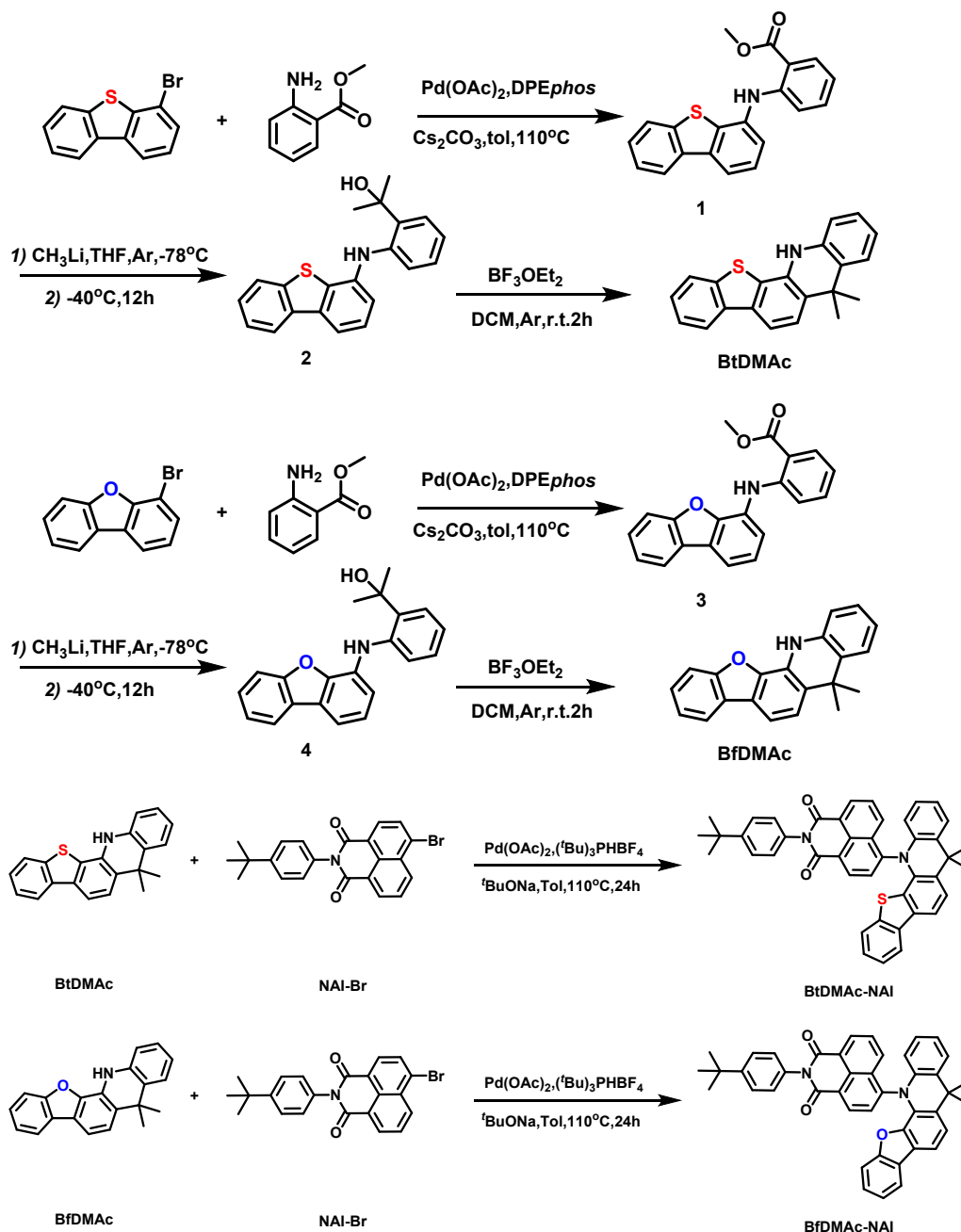
General Information

All reagents were used as received from commercial sources unless otherwise stated. Tetrahydrofuran and toluene were dried by sodium-potassium alloy. ^1H NMR and ^{13}C NMR spectra were measured on a Bruker Advanced II (400 MHz) spectrometers. High resolution mass spectra were measured on a LCQ-Orbitrap Elite (Thermo-Fisher Scientific, Waltham, MA, USA) mass spectrometer. Differential scanning calorimetry (DSC) was performed on a NETZSCH DSC 200 PC unit at a heating rate of $10\text{ }^\circ\text{C min}^{-1}$ from room temperature to $300\text{ }^\circ\text{C}$ under argon. The glass transition temperature (T_g) was determined from the second heating scan. Thermogravimetric analysis (TGA) was undertaken with a NETZSCH STA 449C instrument. The thermal stability of the samples under a nitrogen atmosphere was determined by measuring their weight loss while heating at a rate of $10\text{ }^\circ\text{C min}^{-1}$ from room temperature to $600\text{ }^\circ\text{C}$. Cyclic voltammetry (CV) was carried out in dichloromethane (DCM) at room temperature with a CHI voltammetric analyser. Tetrabutylammonium hexafluorophosphate (TBAPF₆) (0.1 M) was used as the supporting electrolyte. The conventional three-electrode configuration consists of a platinum working electrode, a platinum wire auxiliary electrode, and an Ag wire pseudo-reference electrode with ferrocenium–ferrocene (Fc^+/Fc) as the internal standard. Cyclic voltammograms were obtained at scan rate of 100 mV s^{-1} . Formal potentials are calculated as the average of cyclic voltammetric anodic and cathodic peaks.

Materials Synthesis:

All reagents were used as received from commercial sources and used as received unless otherwise stated.

6-Bromo-2-(4-(*tert*-butyl)phenyl)-1*H*-benzo[*de*]isoquinoline-1,3(2*H*)-dione (NAI-Br) were synthesized according to the literature method.¹



Scheme S1 Synthetic routes of the fused donors and TADF emitters

Synthesis of methyl 2-(dibenzo[*b,d*]thiophen-4-ylamino)benzoate: (1) A mixture of methyl 4-bromodibenzothiophene (2.36 g, 10 mmol), Methyl anthranilate (2.6 mL, 20 mmol), $\text{Pd}(\text{OAc})_2$ (110mg, 0.5mmol), DPEphos (270 mg, 0.5 mmol), toluene (50 mL) and cesium carbonate (3.26 g, 10 mmol) were added into a flask and heated at 110°C under argon overnight. After cooling to room temperature, the reaction mixture was poured into water and extracted with chloroform. The extracted solution was dried over anhydrous Na_2SO_4 . After the removal of the solvent using vacuum evaporator, the residue was purified by column chromatography on silica gel using DCM/petroleum

(1:3 v/v) as the eluent to give a white powder (3.01 g, 9.02 mmol). Yield: 90%. ¹H NMR (400MHz, CDCl₃) δ(ppm): 9.70 (s, 1H), 8.23-8.09 (m, 1H), 8.02 (dd, *J* = 8.1, 1.6 Hz, 1H), 7.96 (dd, *J* = 6.8, 2.0 Hz, 1H), 7.86-7.79 (m, 1H), 7.51-7.41 (m, 4H), 7.34-7.27 (m, 1H), 7.09 (dd, *J* = 8.5, 0.7 Hz, 1H), 6.78 (ddd, *J* = 8.1, 7.2, 1.1 Hz, 1H), 3.95 (s, 3H).

¹³C NMR (100MHz, CDCl₃) δ(ppm): 169.01, 147.51, 139.14, 137.24, 136.11, 135.54, 135.22, 134.12, 131.58, 126.88, 125.37, 124.46, 122.96, 121.82, 120.50, 117.62, 117.58, 114.66, 112.06, 51.96.

Synthesis of 2-(2-(dibenzo[*b,d*]thiophen-4-ylamino)phenyl)propan-2-ol: (2) Under argon to a stirred solution of 2-(dibenzo[*b,d*]thiophen-4-ylamino)benzoate (**1**, 2.00 g, 6 mmol) in dry THF (20 mL) at -78 °C was added a 1.3M solution of methyllithium in diethyl ether (20 mL, 26 mmol) dropwise over 30 minutes. After the mixture was stirred for 1 hour at -78 °C, the mixture was raised to -40 °C and stirred for additional 10 hours. The reaction mixture was then poured into ice water and extracted with EtOAc. The solvent was removed using vacuum evaporator to get a white powder. The crude product was used directly without further purification.

Synthesis of 5,5-dimethyl-5,13-dihydrobenzo[4,5]thieno[3,2-*c*]acridine (BTDMAc): In an oven-dried flask the crude 2-(2-(dibenzo[*b,d*]thiophen-4-ylamino)phenyl)propan-2-ol product (**2**, 1.67 g, 5 mmol) was dissolved in 200 mL dry DCM under argon. Several drops of Boron trifluoride etherate was added. The reaction was monitored by TLC. After the reaction was completed after 4 hours, the mixture was diluted with ice water (20 mL) and extracted with extracted with chloroform. The extracted solution was dried over anhydrous Na₂SO₄. After the removal of the solvent using vacuum evaporator, the residue was purified by column chromatography on silica gel using DCM/petroleum (1:5 v/v) as the eluent to give a white powder (1.32 g, 4.12 mmol). Yield: 82%. ¹H NMR (400MHz, CDCl₃) δ(ppm): 8.20-8.03 (m, 1H), 7.94-7.82 (m, 1H), 7.79-7.62 (m, 1H), 7.52 (d, *J* = 8.2 Hz, 1H), 7.49-7.40 (m, 3H), 7.16 (td, *J* = 7.9, 1.2 Hz, 1H), 6.98 (t, *J* = 7.3 Hz, 1H), 6.86 (d, *J* = 7.8 Hz, 1H), 6.07 (s, 1H), 1.68 (s, 6H). ¹³C NMR (100MHz, CDCl₃) δ(ppm): 138.38, 137.63, 136.40, 134.80, 132.94, 129.27, 126.94, 126.50, 126.36, 126.03, 124.71, 123.60, 123.06, 121.86, 121.40, 114.23, 113.91, 113.80, 36.50, 31.74. HRMS (ESI) *m/z* calcd for C₂₁H₁₈NS⁺ (M+H)⁺ 316.11545, found 316.11496.

Synthesis of methyl 2-(dibenzo[*b,d*]furan-4-ylamino)benzoate (3): A similar procedure used for **1** was carried out but with 4-bromodibenzofuran (2.47 g, 10 mmol) instead of 4-bromodibenzothiophene. The crude product was purified by column chromatography on silica gel using DCM/petroleum (v/v 1:3) as the eluent to give a white powder (2.91 g, 9.18 mmol). Yield: 92%. ¹H NMR (400MHz, CDCl₃) δ(ppm): 9.81 (s, 1H), 8.03 (dd, *J* = 8.0, 1.6 Hz, 1H), 7.96 (dd, *J* = 7.7, 0.6 Hz, 1H), 7.70 (dd, *J* = 7.7, 1.0 Hz, 1H), 7.60 (d, *J* = 8.2 Hz, 1H), 7.54-7.41 (m, 2H), 7.40-7.28 (m, 3H), 7.23 (d, *J* = 0.8 Hz, 1H), 6.81 (ddd, *J* = 8.1, 7.1, 1.1 Hz, 1H), 3.96 (s, 3H). ¹³C NMR (100MHz, CDCl₃) δ(ppm): 169.01, 156.02, 149.03, 147.23, 134.14, 131.60, 127.24, 126.06, 125.52, 124.48, 123.18, 122.84, 120.75, 119.57, 117.69, 115.55, 114.56, 112.52, 112.05, 51.96.

HRMS (ESI) *m/z* calcd for C₂₀H₁₆NO₃⁺ (M+H)⁺ 318.11247, found 318.11234.

Synthesis of 2-(2-(dibenzo[*b,d*]furan-4-ylamino)phenyl)propan-2-ol (4): A similar procedure used for **2** was carried out but with **3** (1.92 g, 6 mmol) instead of **2**. The reaction mixture was poured into ice water and extracted with EtOAc. The solvent was removed using vacuum evaporator to get a yellow powder. The crude product was used directly without further purification.

Synthesis of 5,5-dimethyl-5,13-dihydrobenzofuro[3,2-*c*]acridine (BFDMAc): A similar procedure used for **BTDMAc** was carried out but with **4** (1.59 g, 5 mmol) instead of **3**. The crude product was purified by column chromatography on silica gel using DCM/petroleum (1:5 v/v) as the eluent to give a white powder (1.23 g, 4.11 mmol). Yield: 82% ¹H NMR (400MHz, CDCl₃) δ(ppm): 7.95-7.89 (m, 1H), 7.58 (d, *J* = 8.2 Hz, 1H), 7.50-7.29 (m, 5H), 7.16 (td, *J* = 7.8, 1.3 Hz, 1H), 6.97 (t, *J* = 7.4 Hz, 1H), 6.87 (d, *J* = 7.8 Hz, 1H), 6.73 (s, 1H), 1.68 (s, 6H). ¹³C NMR (100MHz, CDCl₃) δ(ppm): 156.27, 143.05, 137.56, 129.13, 127.49, 126.95, 126.60, 126.05, 124.92, 124.41, 122.86, 122.26, 121.16, 120.82, 120.34, 114.05, 111.60, 111.50, 36.57, 31.65. HRMS (ESI) *m/z* calcd for C₂₁H₁₈NO⁺ (M+H)⁺ 300.13829, found 300.13864.

Theoretical calculation:

The optimal molecular geometry was calculated using the density functional theory (DFT) with Gaussian 09. Ground state geometry optimization was performed using the B3LYP exchange-correlation functional, the def2-SVP basis set and the density functional dispersion correction with Becke-Johnson damping [DFT-D3(BJ)]. The excitation energies were calculated by employing the gap-tuned range-separated LC-BLYP functional with the def2-SVP basis set.

Photophysical Characterization:

Synthesized compounds were subject to purification by temperature-gradient sublimation in high vacuum before use in subsequent studies. Thin films for photophysical characterization were prepared by thermal evaporation on quartz substrates at 1-2 Å/sec in a vacuum chamber with a base pressure of $<10^{-6}$ torr. Absorption spectra were characterized by a UV-vis-NIR spectrophotometer (UV -2700, Shimadzu). Photoluminescence (PL) spectra, photoluminescence quantum yields (Φ_{PL}), and phosphorescence spectra were characterized by a spectrofluorimeter (FluoroMax-P, Horiba Jobin Yvon Inc. or F-4600, Hitachi Inc.). PLs of thin films or dilute solutions were determined using these spectrofluorimeters equipped with a calibrated integrating sphere. During the Φ_{PL} measurements, the integrating sphere was purged with pure and dry nitrogen to keep the environment inert. The selected monochromatic excitation light was used to excite samples placed in the calibrated integrating sphere. By comparing the spectral intensities of the monochromatic excitation light and the PL emission, the PL quantum yields were determined. Phosphorescence spectra of thin films were conducted at 77 K (the liquid nitrogen temperature) by these spectrofluorimeters equipped with a microsecond flash lamp as the pulsed excitation source. A 10 ms delay time was inserted between the pulsed excitation and the collection of the emission spectrum. Time-resolved PL (PL decay curves) was measured by monitoring the decay of the intensity at the PL peak wavelength using the time-correlated single-photon counting fluorescence lifetime system, FLS920 of Edinburgh Instruments using a picosecond pulsed UV-LASTER (LASTER377) as the excitation source.

Device fabrication and measurement:

All organic materials used in experiments (except for the TADF emitters) were purchased from Lumtec, Inc. All compounds were subjected to temperature-gradient sublimation under high

vacuum before use. OLEDs were fabricated on the ITO-coated glass substrates with multiple organic layers sandwiched between the transparent bottom indium-tin-oxide (ITO) anode and the top metal cathode. All material layers were deposited by vacuum evaporation in a vacuum chamber with a base pressure of $\leq 10^{-6}$ torr. The deposition system permits the fabrication of the complete device structure in a single vacuum pump-down without breaking vacuum. The deposition rate of organic layers was kept at 0.1-0.2 nm/s. The doping was conducted by co-evaporation from separate evaporation sources with different evaporation rates. The active area of the device is $1 \times 1 \text{ mm}^2$, as defined by the shadow mask for cathode deposition. The current-voltage-brightness (I-V-L) characterization of the light-emitting devices was performed with a source-measurement unit (SMU) and a spectroradiometer (DMS 201, AUTRONIC-MELCHERS GmbH). EL spectra of devices were collected by a calibrated CCD spectrograph. The angular dependence of EL intensities (and spectra) was measured by a calibrated goniometric spectroradiometer (DMS 201, AUTRONIC-MELCHERS GmbH). The external quantum efficiencies of devices were determined by collecting the total emission fluxes with a calibrated integrating-sphere measurement system and by measuring the angular distribution of the emission spectra and intensities.

Analyses of Rate Constants

The rate constants were analyzed according to the literature method² with the assumption that $k_{RISC} \gg k_{r,T} + k_{nr,T}$, i.e. almost complete harvesting of triplet excitons to singlets and usual $k_p \gg k_d$

$$k_{RISC} \approx \frac{k_p k_d \Phi}{k_{r,s}} \quad (S1)$$

$$k_{ISC} \approx \frac{k_p k_d \Phi_d}{k_{RISC} \Phi_p} \quad (S2)$$

Where k_p and k_d represent the decay rate constants for prompt and delayed fluorescence, respectively. They can be experimentally determined from prompt and delayed fluorescence decay time constants (τ_p and τ_d) with a reciprocal relationship. Φ_p and Φ_d represent quantum yields for the prompt and delayed fluorescence components. $k_{r,s}$ were calculated using the Equation 1.

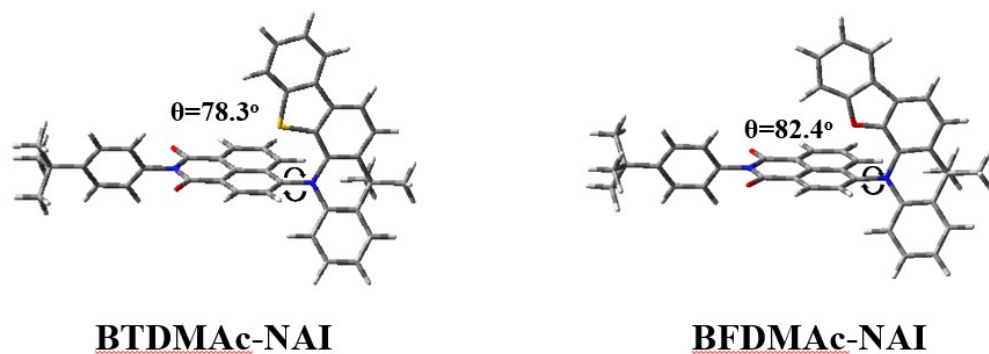
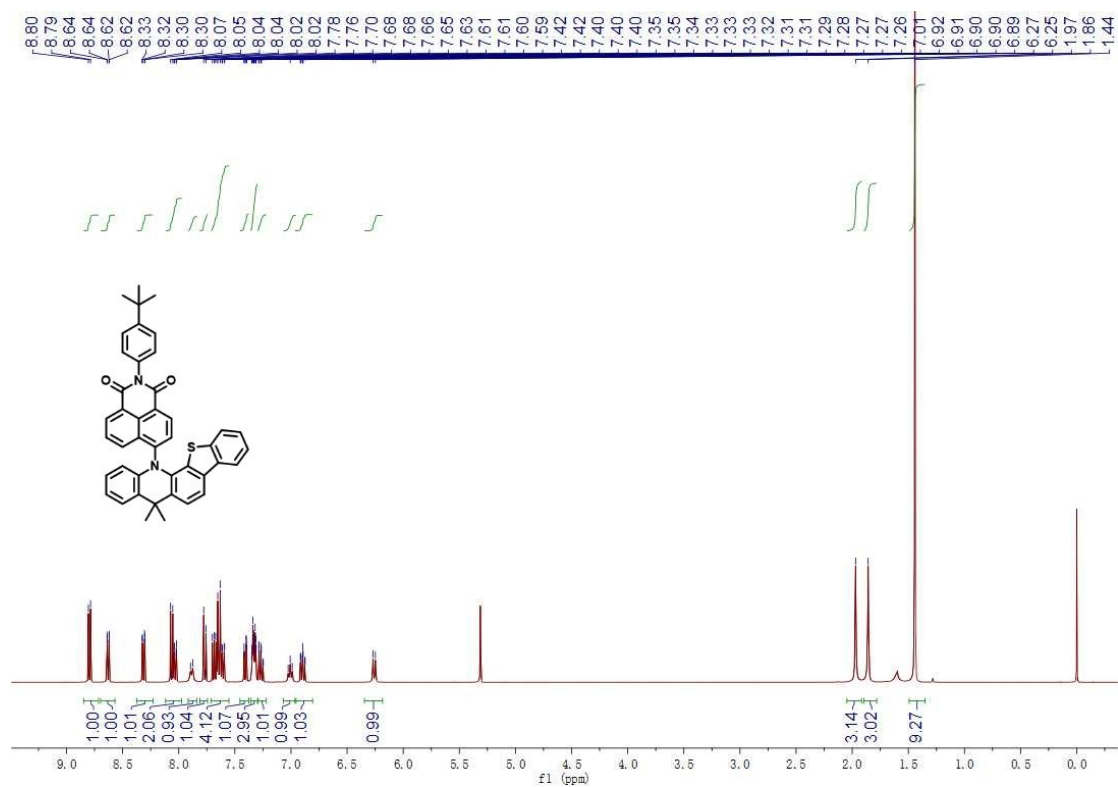


Figure S1. The optimized ground-state geometries of two emitters



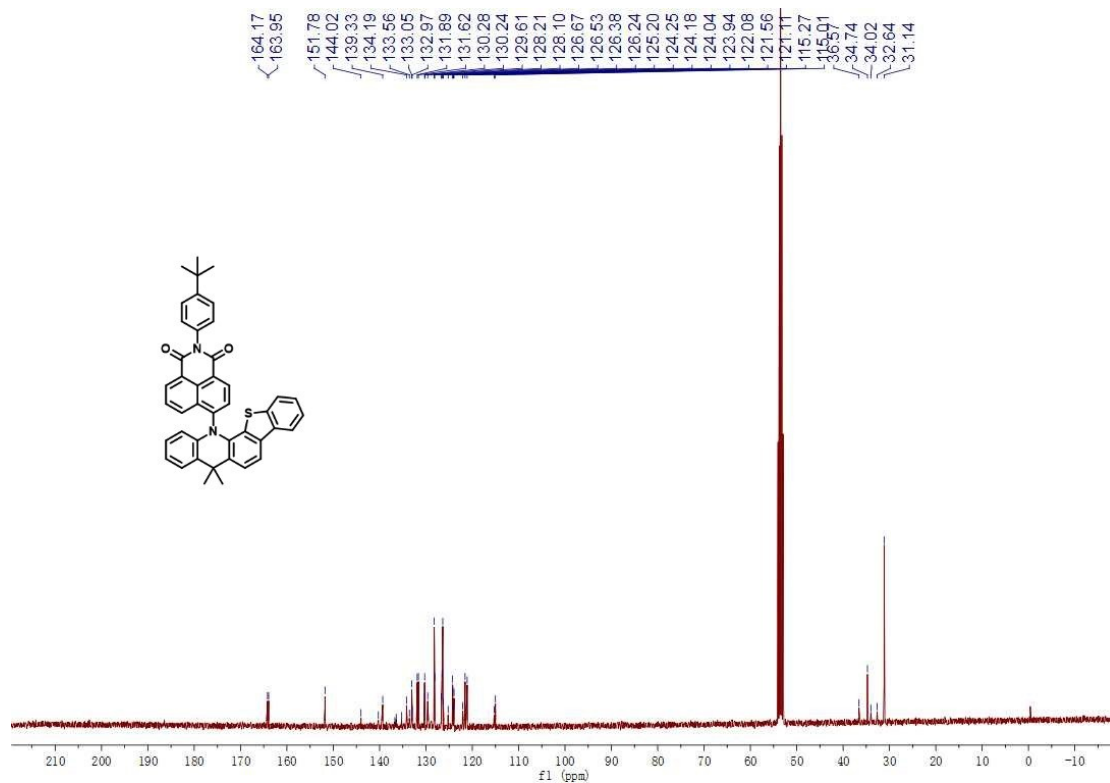


Figure S3. ¹³C spectra of BTDMac-NAI (400 MHz, CD₂Cl₂ + TMS, 25 °C)

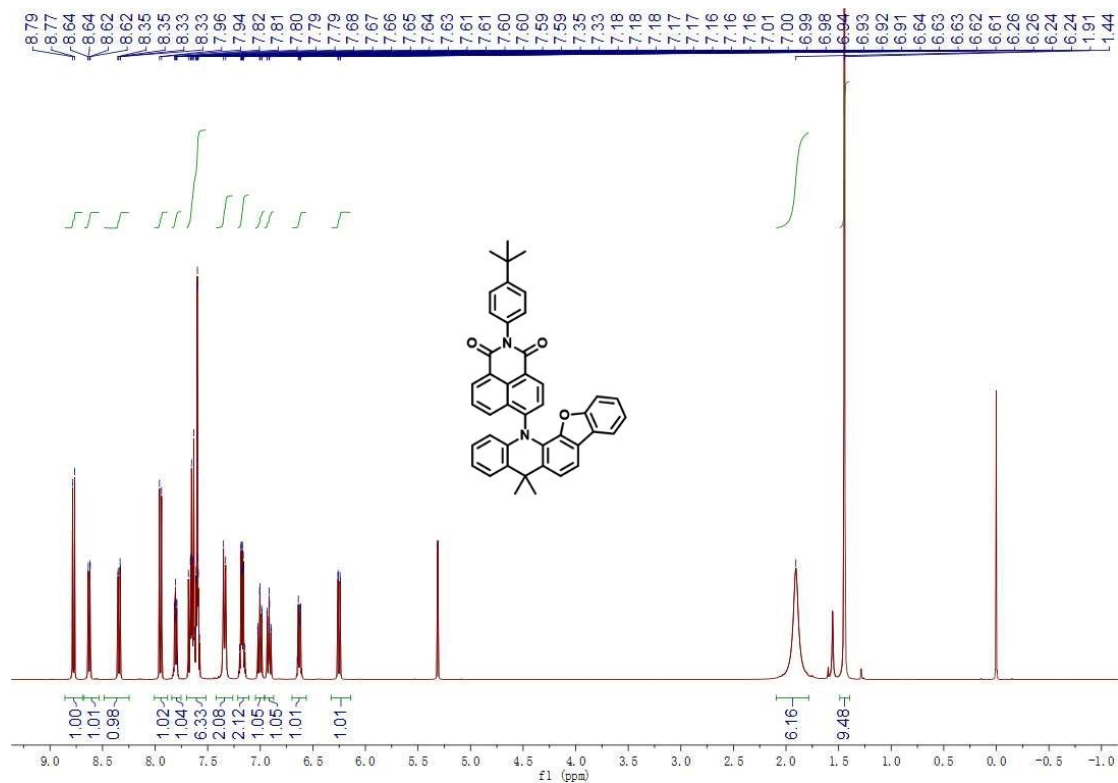


Figure S4. ^1H spectra of BFDMAc-NAI (400 MHz, CD_2Cl_2 + TMS, 25 °C)

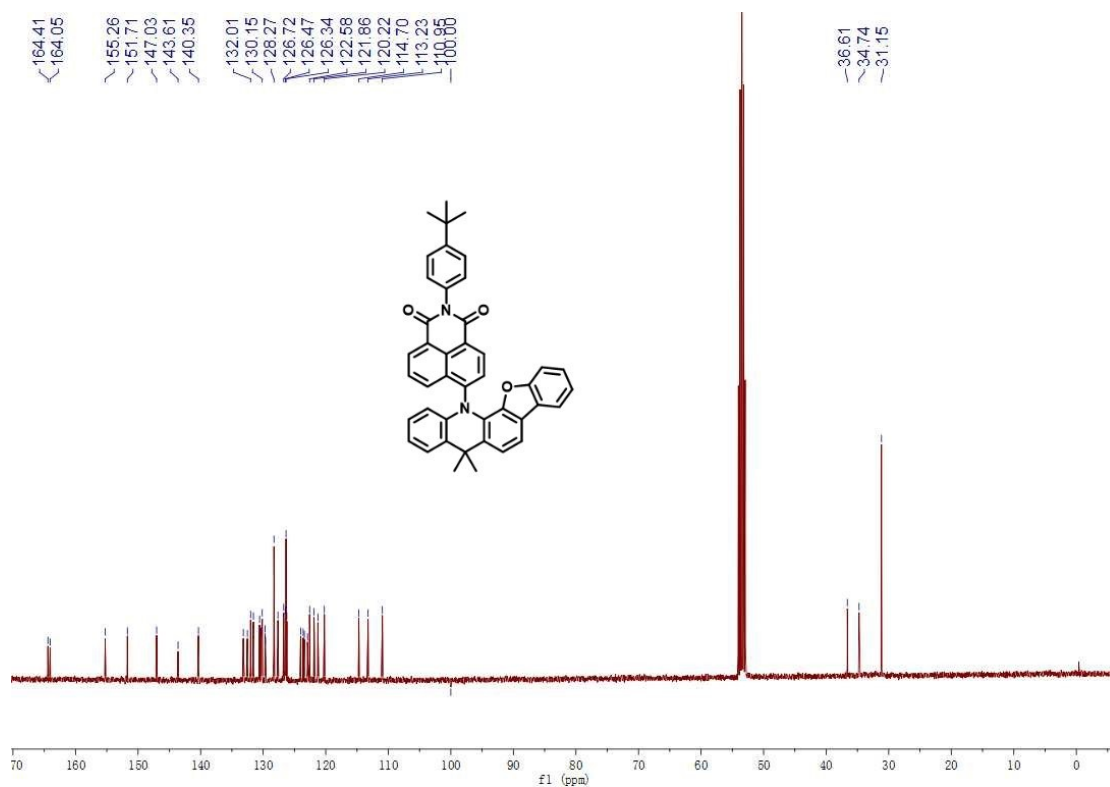


Figure S5. ^{13}C spectra of BFDMAc-NAI (400 MHz, CD_2Cl_2 + TMS, 25 °C)

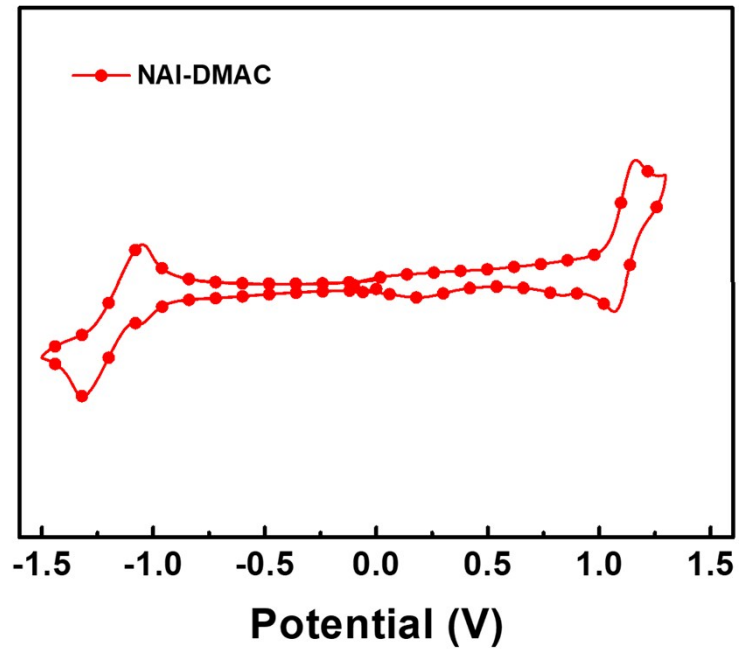


Figure S6. Oxidation and reduction behaviors of NAI-DMAC.

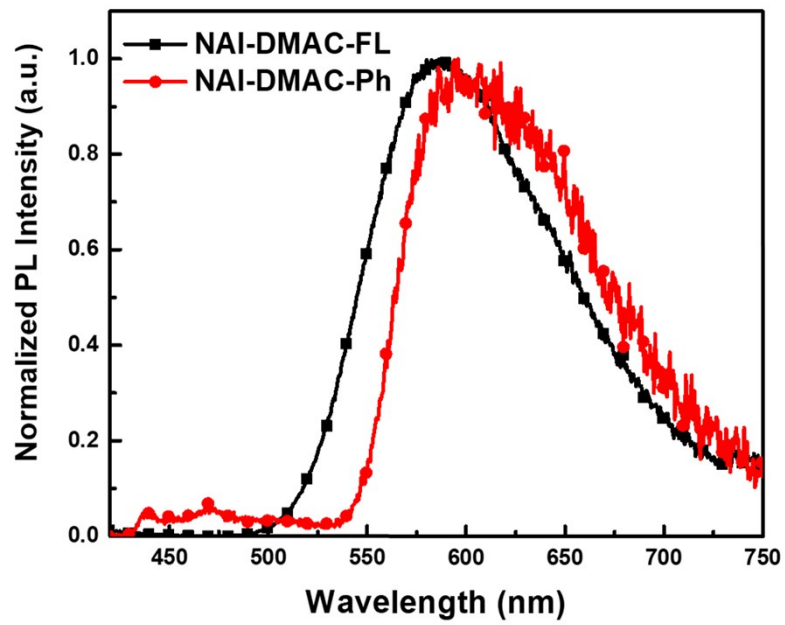


Figure S7. Fluorescence and phosphorescence spectra of NAI-DMAC doped into mCPCN film (1.5 wt%)

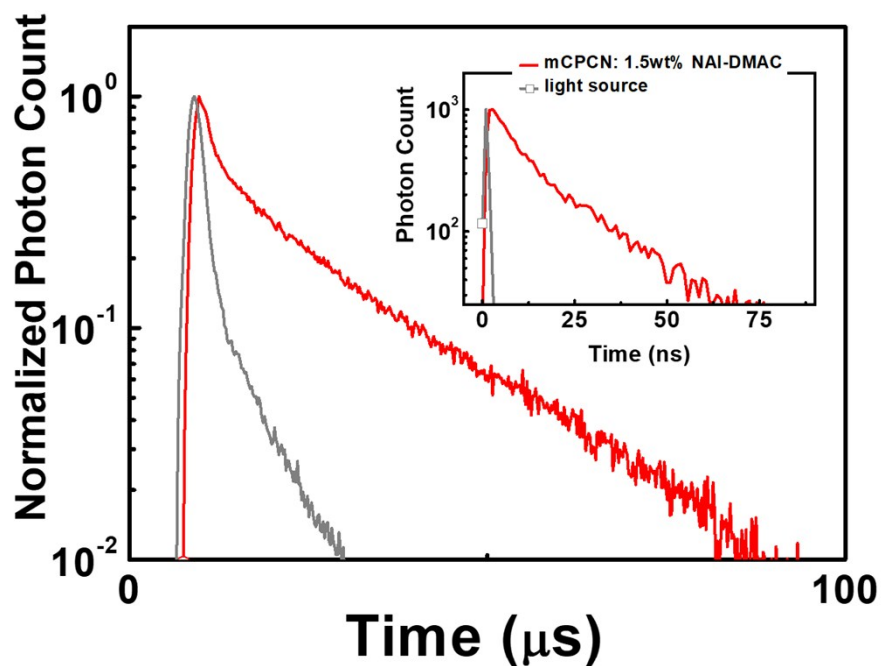


Figure S8. The transient photo-luminescence decay spectra of NAI-DMAC doped into mCPCN film (1.5 wt%) at room temperature.

Table S1. The summary of physical properties of NAI-DMAC

Compound	$\lambda_{\text{abs}}^{\text{a}}$	$\lambda_{\text{PL}}^{\text{b}}$	S_1^{c}	T_1^{d}	$\Delta E_{\text{S}_1\text{T}}^{\text{e}}$	$\tau_{\text{p}}^{\text{f}}$	$\tau_{\text{d}}^{\text{f}}$	Φ^{g}	$\Phi_{\text{p}}/\Phi_{\text{d}}^{\text{h}}$	HOMO ⁱ	LUMO ⁱ
			[eV]	[eV]	[eV]	[ns]	[μs]	[%]	[%]	[eV]	[eV]
NAI-DMAC	353/460	587	2.35	2.31	0.04	12.7	14.7	60	9/51	-5.41	-3.25

^aMeasured in toluene (10^{-5} M) at room temperature. ^bMeasured in doped mCPCN film (1.5 wt%) at room temperature. ^cCalculated from the onset of the fluorescence spectra of NAI-DMAC doped into mCPCN films (1.5 wt%) at room temperature. ^dCalculated from the onset of the phosphorescence spectra of NAI-DMAC doped into mCPCN films (1.5 wt%) at 77K. ^e $\Delta E_{\text{S}_1\text{T}} = S_1 - T_1$. ^fThe prompt and delayed fluorescence lifetimes of NAI-DMAC doped into mCPCN films (1.5 wt%) at room temperature. ^gThe total PLQY of NAI-DMAC doped into mCPCN films (1.5 wt%) under oxygen-free conditions at room temperature. ^hThe prompt and delayed fluorescence PLQY under oxygen-free conditions. ⁱHOMO/LUMO level calculated from the oxidation/reduction half-wave potentials.

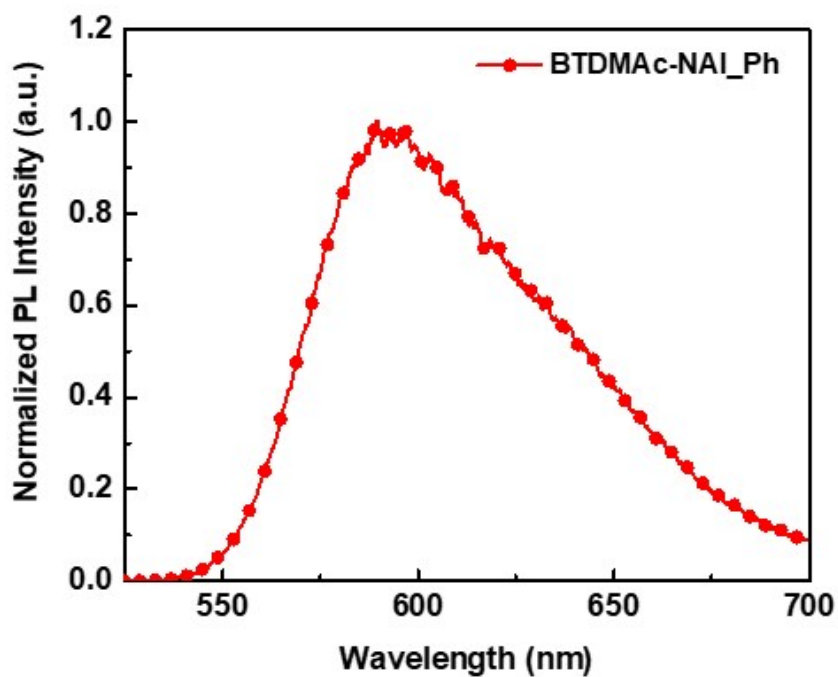


Figure S9. Phosphorescence spectra of BTDMAc-NAI in toluene (10^{-5} M)

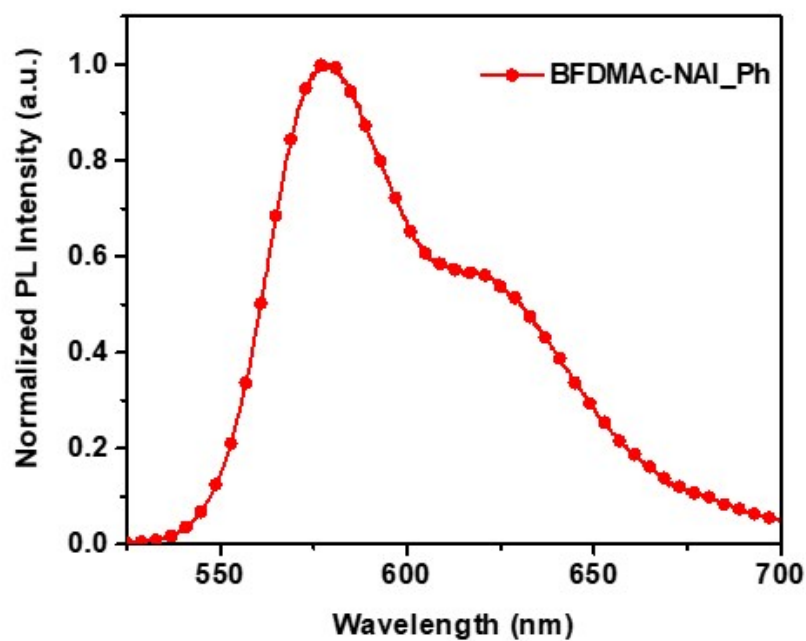


Figure S10. Phosphorescence spectra of BFDMAc-NAI in toluene (10^{-5} M)

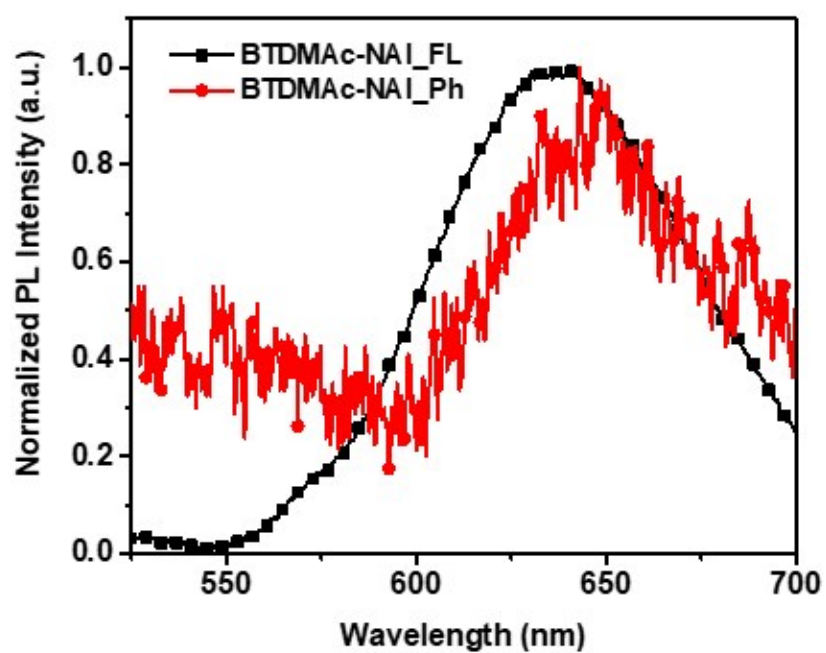


Figure S11. Fluorescence and phosphorescence spectra of BTDMAc-NAI in neat film.

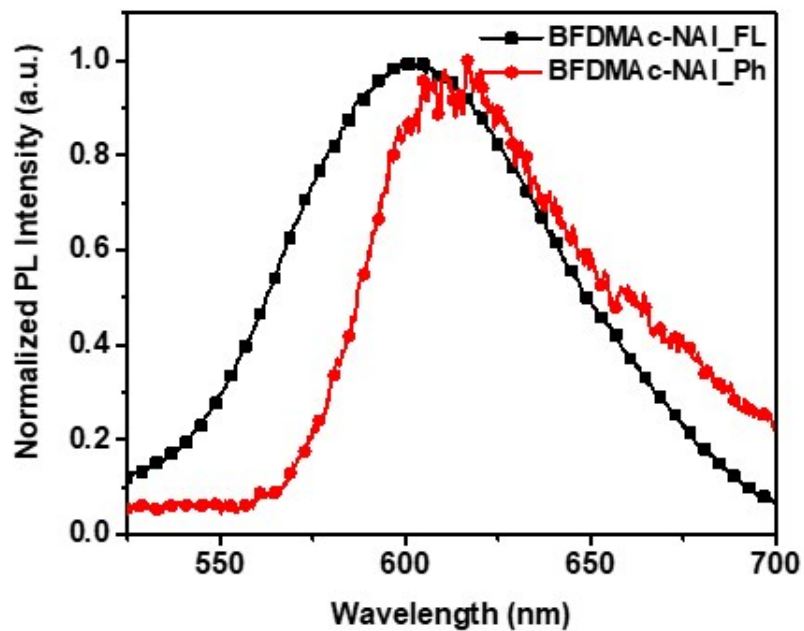


Figure S12. Fluorescence and phosphorescence spectra of BFDMAc-NAI in neat film.

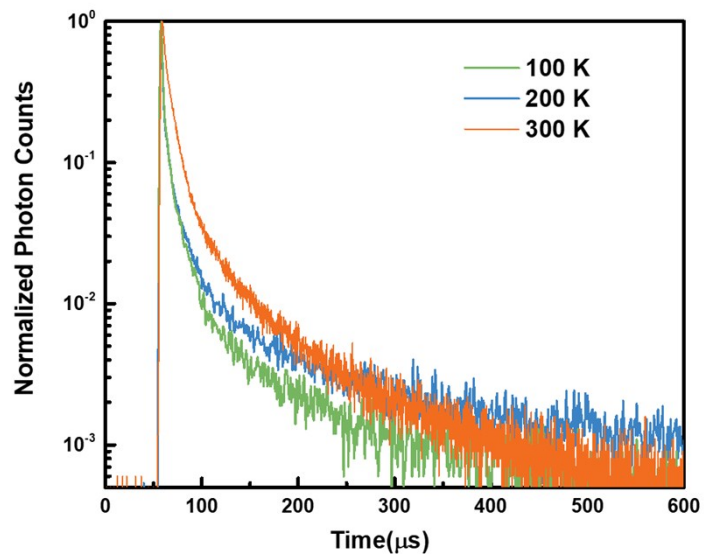


Figure S13. The transient photo-luminescence decay spectra of BTDMAc-NAI doped into mCPCN film (1.5 wt%) at various temperatures.

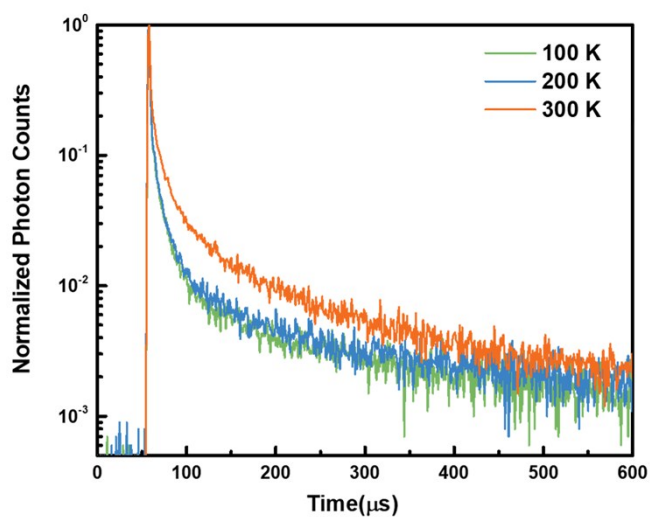


Figure S14. The transient photo-luminescence decay spectra of BFDMAc-NAI doped into mCPCN film (1.5 wt%) at various temperatures.

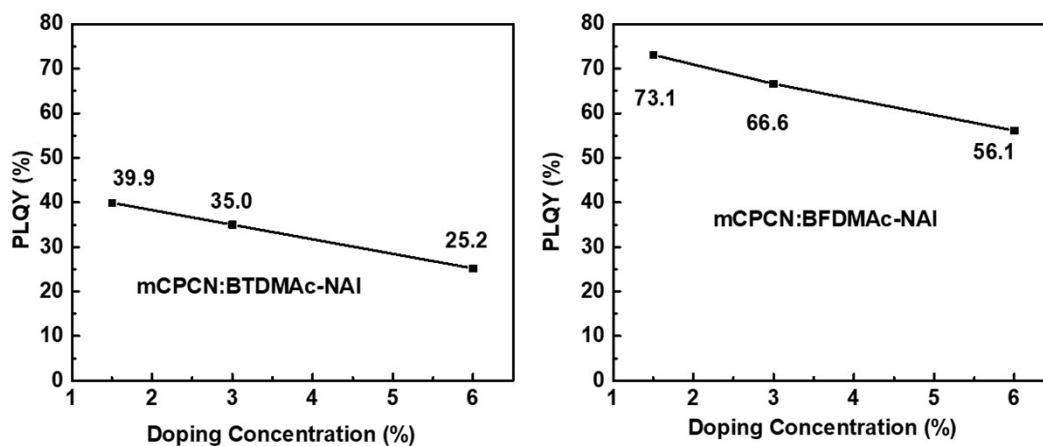


Figure S15. Photoluminescence quantum yield versus doping concentrations of two emitters

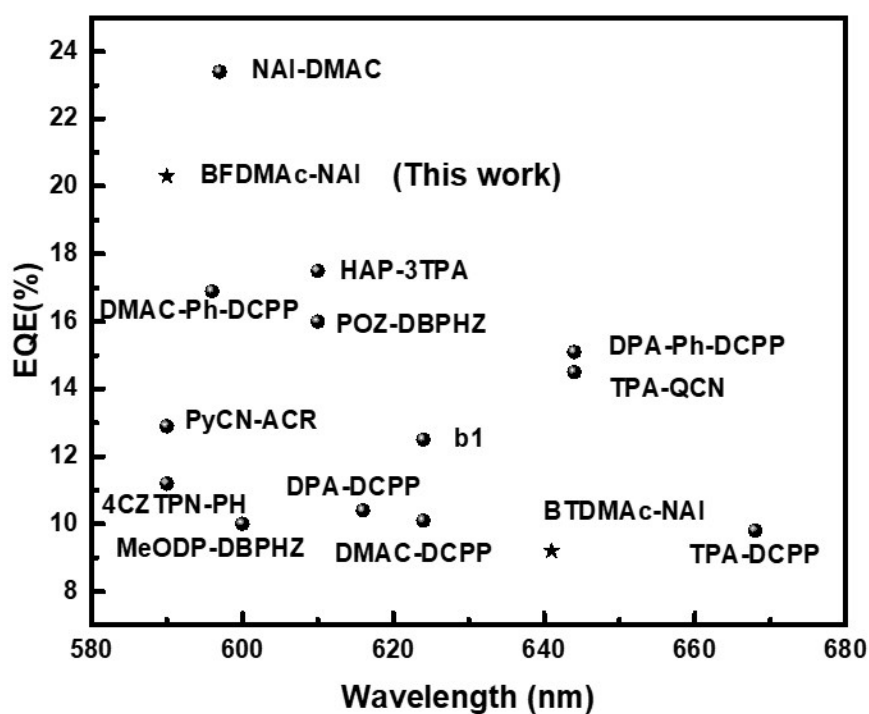


Figure S16. EQE versus EL peak wavelength of high efficiency orange-red TADF OLEDs reported in the literature.²⁻⁸

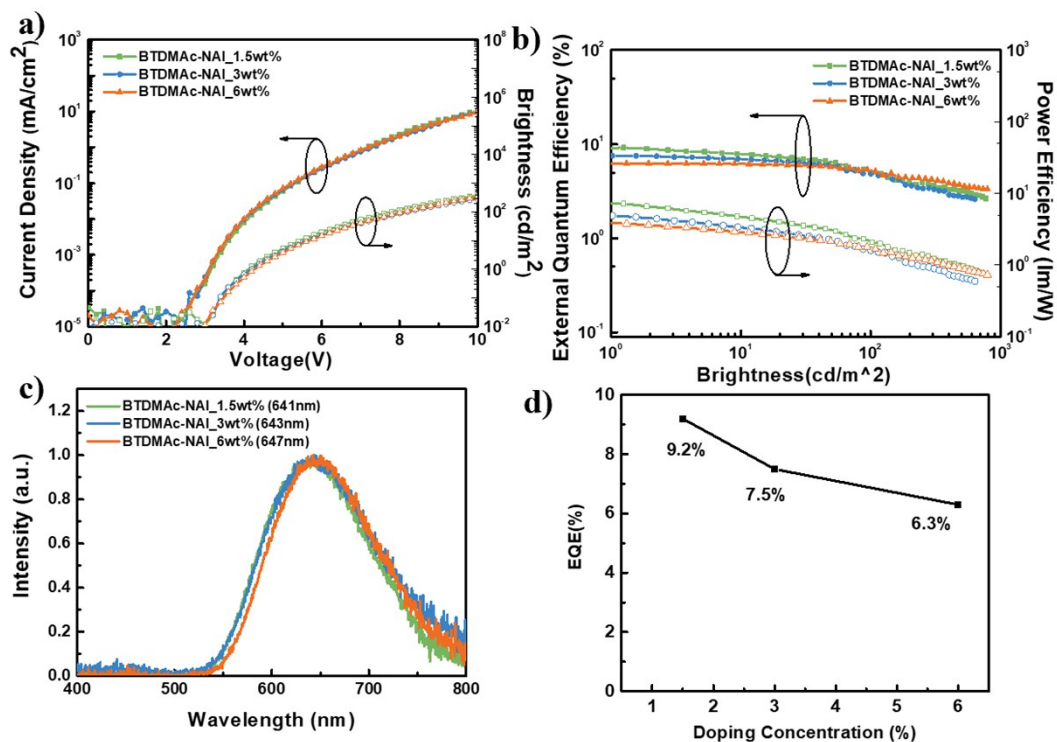


Figure S17. a-c) Luminance-voltage-current density curves, external quantum efficiency and power efficiency versus luminance characteristics for devices based on emitting layers with different doping concentrations of BTDMac-NAI. d) EQE versus doping concentration of devices based on BTDMac-NAI

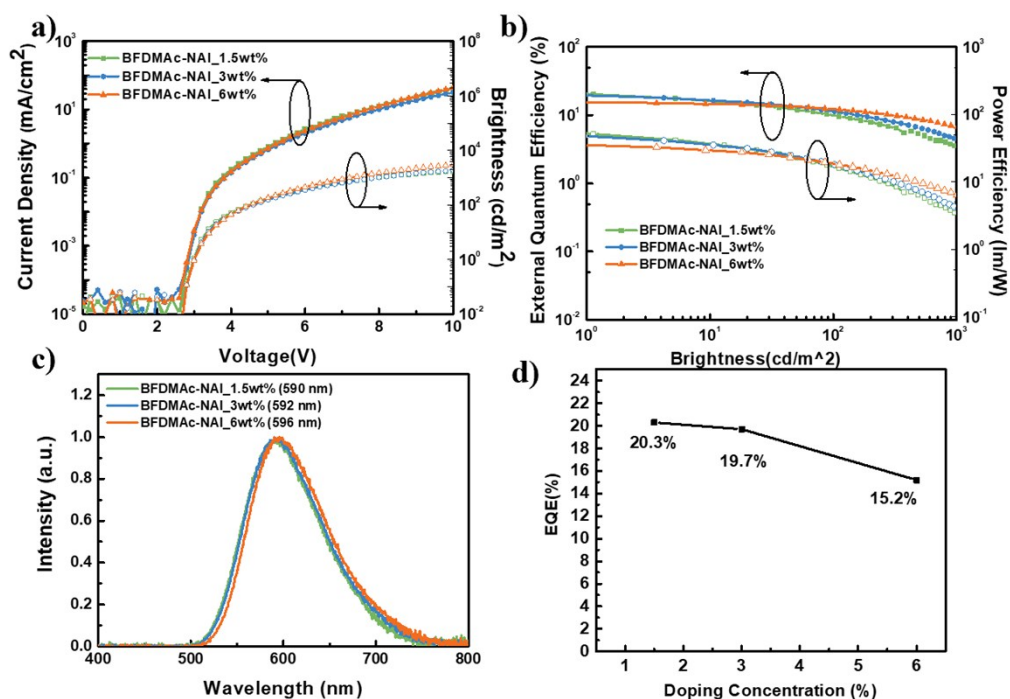


Figure S18. a-c) Luminance-voltage-current density curves, external quantum efficiency and power efficiency versus luminance characteristics for devices based on emitting layers with different doping concentrations of **BFDMAc-NAI**. d) EQE versus doping concentration of devices based on **BFDMAc-NAI**.

Reference

1. G. Tu, Q. Zhou, Y. Cheng, Y. Geng, L. Wang, D. Ma, X. Jing and F. Wang, *Synthetic Metals*, 2005, **152**, 233-236.
2. K.-C. Pan, S.-W. Li, Y.-Y. Ho, Y.-J. Shiu, W.-L. Tsai, M. Jiao, W.-K. Lee, C.-C. Wu, C.-L. Chung, T. Chatterjee, Y.-S. Li, K.-T. Wong, H.-C. Hu, C.-C. Chen and M.-T. Lee, *Adv. Funct. Mater.*, 2016, **26**, 7560-7571.
3. H. Uoyama, K. Goushi, K. Shizu, H. Nomura and C. Adachi, *Nature*, 2012, **492**, 234-238.
4. S. Wang, Z. Cheng, X. Song, X. Yan, K. Ye, Y. Liu, G. Yang and Y. Wang, *ACS Appl. Mater. Interfaces*, 2017, **9**, 9892-9901.
5. X. Cai, X. Li, G. Xie, Z. He, K. Gao, K. Liu, D. Chen, Y. Cao and S.-J. Su, *Chem. Sci.*, 2016, **7**, 4264-4275.
6. P. Data, P. Pander, M. Okazaki, Y. Takeda, S. Minakata and A. P. Monkman, *Angew. Chem. Int. Ed.*, 2016, **55**, 5739-5744.
7. J. Li, T. Nakagawa, J. MacDonald, Q. Zhang, H. Nomura, H. Miyazaki and C. Adachi, *Adv. Mater.*, 2013, **25**, 3319-3323.
8. M. Okazaki, Y. Takeda, P. Data, P. Pander, H. Higginbotham, A. P. Monkman and S. Minakata, *Chem. Sci.*, 2017, **8**, 2677-2686.
9. W. Zeng, H.-Y. Lai, W.-K. Lee, M. Jiao, Y.-J. Shiu, C. Zhong, S. Gong, T. Zhou, G. Xie, M. Sarma, K.-T. Wong, C.-C. Wu and C. Yang, *Adv. Mater.*, 2018, **30**, 1704961.